JOURNAL OF GEOPHYSICAL RESEARCH, VOL. 114, A10208, doi:10.1029/2009JA014257, 2009

Plasmoid-like structures in multiple X line Hall MHD reconnection

C. X. Liu,[1] S. P. Jin,[1] F. S. Wei,[2] Q. M. Lu,[1] and H. A. Yang[3]

Received 16 March 2009; revised 19 June 2009; accepted 30 June 2009; published 21 October 2009.

[1] Driven by a waveform inflow, multiple X line reconnection is initiated in a long current layer, and the plasmoids are bound between two neighboring reconnection sites. We investigate the behaviors of the plasmoid-like structures in the absence and presence of an initial guide field B_{y0} normalized by B_0 (B_0 is the initial intensity of B_x field at the top and bottom boundaries of the simulation domain) using a Hall magnetohydrodynamic (MHD) code. For the case with $B_{y0} = 0$ the profiles of the out-of-plane B_y component are the bipolar signature or the bipolar wavelike signature which is caused by Hall effect and independent of the external mechanism. Such B_y features are in line with the observed signature of a closed-loop-like plasmoid in the magnetotail. The bipolar and fluctuation signatures of B_y have an asymmetric feature in the presence of a small B_{y0}(= 0.1), and the B_y profile becomes a positive signature as B_{y0} reaches or exceeds 0.3. In the case of B_{y0} = 0.5, a B_y bulge appears in the B_y signature when the enhanced B_y regions caused by Hall effect take place in the plasmoid. The B_y bulge evolves into a peaking signature, whose maximum ($B_y|_{\max}$) is quickly raised and approaches the lobe magnetic field strength. Such a significant enhancement of the B_y component in the central region of the plasmoid might be representative of the observed strong core field in the magnetic flux rope. The present results indicate the following implications: (1) Hall effect and a preexisting cross-tail component B_y are two important factors controlling the occurrence of various plasmoid-like structures in the magnetotail. (2) In the later phase the nonlinear interaction between Hall effect and the B_y flux added by the plasma inflow makes a most important contribution to the growth of the core B_y field.

Citation: Liu, C. X., S. P. Jin, F. S. Wei, Q. M. Lu, and H. A. Yang (2009), Plasmoid-like structures in multiple X line Hall MHD reconnection, *J. Geophys. Res.*, *114*, A10208, doi:10.1029/2009JA014257.

1. Introduction

[2] Plasmoids have been observed in the magnetotail by a number of early spacecraft missions, for example, ISEE [*Moldwin and Hughes*, 1993; *Slavin et al.*, 1989] and Geotail [*Deng et al.*, 2004; *Ieda et al.*, 1998; *Zong et al.*, 1997]. A large number of plasmoids observed in the magnetotail exhibit not only the usual bipolar signature in the north–south magnetic field component B_z, but also a very strong cross-tail magnetic field component B_y (core B_y field) which can approach or exceed the ambient lobe magnetic field in magnitude. Such plasmoids with helical magnetic field structures were called "magnetic flux rope" (MFR) [*Chen et al.*, 2007; *Ieda et al.*, 1998; *Slavin et al.*, 1995]. The dawn-dusk magnetic field B_y in the magnetotail has been found to be well correlated with the interplanetary magnetic field (IMF) B_y component. *Lui* [1984] suggested that about 50% of the IMF B_y component exists in the neutral sheet region. In addition, the other kind of plasmoids detected in the magnetotail reveals the bipolar waveform signatures in both B_z and B_y components [*Deng et al.*, 2004; *Zong et al.*, 1997; *Moldwin and Hughes*, 1992]. They were considered to be plasmoid-like structures with closed-looped magnetic field lines. In the present work the term plasmoid is used for both of MFR and "closed loop" plasmoid.

[3] The formation of plasmoids in the magnetotail can be understood in terms of the multiple X line reconnection (MXR) model proposed to explain the helical magnetic structure in flux transfer events (FTEs) at the dayside magnetopause [*Lee et al.*, 1985]. The Geotail spacecraft encountered an active reconnection diffusion region in the Earth's magnetotail. *Deng et al.* [2004] provided evidence of multiple X line collisionless reconnection on the basis of the following observed features: quadrupole pattern of the out-of-plane B_y component during the passage of a magnetic island, a direction reversal of the electron beams and plasma flow reversal. On 2 October 2003 the observation made by the four Cluster spacecraft showed that the variations of field and flow in the vicinity of magnetotail current sheet

[1]School of Earth and Space Sciences, University of Science and Technology of China, Hefei, China.
[2]State Key Laboratory of Space Weather, Center for Space Science and Applied Research, Chinese Academy of Sciences, Beijing, China.
[3]Space Science Center, University of New Hampshire, Durham, New Hampshire, USA.

0148-0227/09/2009JA014257$09.00

are most consistent with a series of two active reconnection sites bounding an Earthward moving flux rope [*Eastwood et al.*, 2005]. It indicated that reconnection can occur simultaneously at different points in the near-Earth magnetotail current sheet, providing (further) important experimental validation of MXR theories on the mesoscale (tens of ion inertial length) level [*Eastwood et al.*, 2005]. The "time of flight" of the flux rope across the 4 Cluster spacecraft yielded $V_x \sim 700$ km/s and a diameter of ~ 1 R_e [*Slavin et al.*, 2003]. *Lui et al.* [2007] investigated an MFR observed by Cluster during a substorm, and found that the MFR was aligned with its principal axis closely along the dawn-dust direction. A theoretical study [*Drake et al.*, 2005] suggested that electrons gain kinetic energy by reflecting from the contracting "magnetic islands" that form as reconnection proceeds. Recently, *Chen et al.* [2007] provided evidence for the link between energetic electrons and magnetic islands during reconnection in the Earth's magnetotail on the basis of the observation made by the four Cluster spacecraft.

[4] Many attempts have been done to explain the observed strong core field in plasmoids. *Walker and Ogino* [1996] studied the origin and evolution of MFR using a three-dimensional (3-D) global MHD simulation. When there initially was no IMF B_y in the plasma sheet, reconnection led to the formation of plasmoid composed of a quasi-2-D closed magnetic loop structure. For IMF $B_y \neq 0$ initially in the plasma sheet the reconnection immediately led to the formation of an MFR structure [*Walker and Ogino*, 1996]. *Ma et al.* [1994] proposed that the increase in the core magnetic field depends on both the property of the initial configuration and the particular reconnection geometry on the basis of the 2-D and 3-D simulations of various reconnection models. *Sonnerup* [1987] examined the basic properties and motions of flux tubes of the Russell-Elphic type for FTEs at the magnetopause and suggested that in the supercritical case the circumferential magnetic flux is continually fed into the flux tube from the surrounding magnetopause and the helical FTE field lines are formed. A 2.5-D MHD simulation of multiple-plasmoid-like structures in the course of a substorm was carried out by *Jin et al.* [2001]. The results indicated that the occurrence of various magnetic structures in the magnetotail might be related to the different initial distributions of B_y component in the driven reconnection processes. The evolution of the helical topology in the reconnected flux tube was investigated by *Jin and Cui* [2004] in terms of the principle of magnetic helicity. It was found that the concentration of the helicity density h in the core of a flux tube arises from the enhancement of the axial field B_y, which is associated with the continuous addition of B_y flux to the domain. However, the above studies [*Jin et al.*, 2001; *Jin and Cui*, 2004] based on MHD model did not include the effect of Hall current. *Karimabadi et al.* [1999] carried out 2-D and 3-D hybrid simulations that explained the large core field in terms of Hall-generated currents which can naturally lead to core field strength exceeding even the ambient lobe field magnitude. Ion beta and the presence of a preexisting guide field are two important factors controlling the Hall-generated field. Full particle simulations were presented by *Drake et al.* [2006] that suggested that the strength of an ambient guide magnetic field controls whether magnetic reconnection remains steady or becomes bursty. Specifically during antiparallel (component) reconnection the electron current layers that form near the magnetic X line are short (long) and therefore stable (unstable) to the formation of secondary magnetic islands. A fully kinetic simulation showed that the length of the electron diffusion region is observed to increase with time resulting in the formation of an extended electron current sheet, and the electron layer becomes unstable and produces a secondary island in the reconnection with open boundary condition [*Daughton et al.*, 2006]. Besides, the effect of the guide field on the electron acceleration was examined by a particle simulation [*Fu et al.*, 2006].

[5] We derived a 2.5-D Hall MHD code from the multistep implicit scheme [*Hu*, 1989] to study collisionless reconnection problems. For the quasi-steady reconnection with a single X line the following works have been carried out. The driven reconnection processes with various scales were investigated [*Yang and Jin*, 2004]. The single X reconnection with a quadrupolar B_y structure was exhibited in the cases with $L_c/d_i \leq 1.0$ (L_c is the half-thickness of initial current layer, d_i is the ion inertial length). The reconnection rates $\partial A/\partial t \approx 0.15$ and 0.11 in the quasi-steady states for the cases of $L_c/d_i = 0.5$ and 1.0, and they are insensitive to different magnitude of the spatially uniform resistivity. The single X reconnection is transformed into the reconnection with an extended current sheet and the reconnection rate is dramatically reduced as the Hall effect weakens with increasing L_c/d_i. The results from the reconnection process driven by the plasma inflow are compatible with those obtained from the reconnection initiated by magnetic perturbations in the GEM reconnection challenge [*Birn et al.*, 2001]. *Jin et al.* [2005] examined the dependence of the Hall effect on plasma β, and found that the openness of the magnetic separatrix angle is enlarged as β increases and the fine structures of B_y contours with reversed sign emerge as $\beta > 2.0$. The numerical results indicated that these fine structures are attributed to the reversed currents associated with the relative motions between electrons and ions [*Jin et al.*, 2005]. The density depletion layers in magnetic reconnection were explored [*Yang et al.*, 2006]. The simulation results showed not only the density depletions along the magnetic separatrices but also a density dip near the X line and indicated that the Hall effect is responsible for the phenomena of density depletion. On the basis of the comparison between simulation results and Wind observations we argued that the density dip observed by Wind would be distributed around the reconnection X line, rather than along the magnetic separatrix [*Yang et al.*, 2006]. The effects of the initial guide field B_{y0} on the reconnection dynamics were examined by *Yang et al.* [2008]. The openness of the magnetic separatrix angle is slightly reduced, and the features of the reconnection field are substantially altered in the presence of B_{y0}. The reconnection rates($\partial A/\partial t$) at the X line drops from 0.151 to 0.06 as B_{y0} increases from 0 to 4.0 (in unit of B_0, B_0 is the initial intensity of the oppositely directed field component B_x at the top and bottom boundaries), and $\partial A/\partial t$ in the case of $B_{y0} = 1.0$ is about 75% of that in the case of $B_{y0} = 0$. This result is approximate to that in *Huba*'s [2005] simulation where the reconnection is initiated by magnetic perturbations.

[6] In the present work we use a 2.5-dimensional Hall MHD code to investigate the dynamic features of the multiple X line reconnection. In (x, z) plane the opposite-pointing magnetic field lines driven by the plasma inflow approach each other, and as a result the tearing mode instability is triggered and the multiple X line reconnection is initiated in a long current layer. It is found from 2.5-D Hall MHD simulations that the thin current sheet with a sufficient length facilitates the trigger of a tearing mode instability. The behaviors of the plasmoids to be bound between two neighboring reconnection sites, especially the evolving features of out-of-plane B_y component associated with Hall effect are explored in the absence and presence of an initial guide field B_{y0}. The numerical results exhibit the observed features of two types of plasmoid-like structures in the magnetotail. The factors controlling the occurrence of various plasmoid-like structures will be discussed.

2. Simulation Model

[7] A magnetic flux function $A(x, z, t)$ is introduced by the equation

$$\mathbf{B} = \nabla \times \left(A\mathbf{e}_y\right) + B_y\mathbf{e}_y. \tag{1}$$

We assume that the x coordinate of a right-handed Cartesian coordinate system is in the tailward direction, the z coordinate is perpendicular (northward) to the plasma sheet, and y coordinate is in the dusk-dawn direction. A Harris current sheet equilibrium solution is chosen as the initial state. At $t = 0$, the magnetic field is

$$B_x(x,z) = -B_0 \tanh(z/L_c), \quad B_z(x,z) = 0, \tag{2}$$

the corresponding magnetic flux function is given by

$$A(x,z) = A_0 \ln(\cosh(z/L_c)). \tag{3}$$

[8] The static isothermal equilibrium state is given by $V_x(x, z) = V_y(x, z) = V_z(x, z) = 0$, $T(x, z) = T_0$ and $\rho(x, z) = \rho_0 + \rho_c\mathrm{sech}^2(z/L_c)$, and ρ_c is determined by $RT_0\rho_c = B_0^2/8\pi$ (R is gas constant) and $\rho_c = 2.0\rho_0$. To facilitate the trigger of a tearing mode instability and the formation of multiple X line reconnection, the half width of the initial current sheet L_c was set as $0.04\mathrm{L}_0$ (i.e., $L_c = 0.04\mathrm{L}_0$, L_0 is the half length of simulation domain in z direction). The initial Harris sheet equilibrium is not modified by the addition of a uniform out-of-plane magnetic field component B_{y0}, and so the cases with the guide field B_{y0} ranging from 0 to 1.2 (in unit of B_0, B_0 is the initial value of B_x field at the top and bottom boundaries) are investigated in this simulation.

[9] On the basis of the Hall MHD approximation, the generalized Ohm's law, including the Hall current and scalar electron pressure gradient terms, is combined with Faraday's induction equation. The 2.5-D Hall MHD equations are written in dimensionless forms which are given by *Jin et al.* [2005] and *Yang et al.* [2006]. The length, magnetic field strength, density, temperature, magnetic flux function, velocity and time are scaled by L_0, B_0, ρ_0, T_0, $A_0 = B_0L_0$, $V_A = B_0/\sqrt{\rho_0}$ and $\tau_A = L_0/V_A$, respectively. And the factor $(4\pi)^{1/2}$ is involved in the unit of B_0, so that $1/4\pi$ does not appear in Lorentz force terms. The dimensionless parameters χ_m, K_H, K_P are given by

$$\chi_m = \frac{\eta}{V_AL_0},\ K_H = \frac{d_i}{L_0},\ K_P = \frac{\beta}{2}\frac{d_i}{L_0}, \tag{4}$$

where η is the plasma resistivity and $\beta = P_0/(B_0^2/2)$ is the ratio of plasma pressure to magnetic pressure outside the current sheet. In the present study, the resistivity η is assumed to be uniform and the Lundquist number S ($= L_0V_A/\eta = 1/\chi_m$) is set as 2500. The other parameters are taken as follows: $T_0 = 1.44 \times 10^7$K, $B_0 = 20$ nT, $\rho_0 = 3.34 \times 10^{-25}$ g/cm^3 (corresponding to $n_{ion} = 0.2$ protons/cm^3), $d_i = c/\omega_{pi} = c/\sqrt{\frac{4\pi e^2 n_0}{m_i}} = 509$ km, $L_0 = 5d_i$ and $\beta = 0.5$.

[10] The numerical computation is carried out in the whole simulation domain which extends from 0 to L_x in the x direction and from $-L_z$ to L_z in the z direction. To examine the behaviors of multiple X line reconnection, the long domain ($L_x = 12$ in unit of L_0) is employed in the runs presented here. Along the left boundary ($x = 0$) and right boundary ($x = L_x = 12$), ρ, V_x, V_y, V_z, B_y, and T are determined by linear extrapolation. For the magnetic flux function $A(x, z, t)$, we choose $\partial^2A/\partial x^2 = 0$ (i.e., $\partial B_z/\partial x = 0$) at the left and right boundaries. Along the top boundary ($z = L_z = 1$) and bottom boundary ($z = -L_z = -1$), the parameters ρ, T, B_y, V_x, and V_y are maintained at their initial values, and $\partial^2A/\partial z\partial t$ is chosen to be zero (i.e., $\partial B_x/\partial t = 0$). In order to simulate the situation of driven reconnection with multiple X line, the inflows V_z (in unit of V_A) are imposed at the top and bottom boundaries,

$$V_z = \mp\{V_1 \cos[(x/L_{cx} - 5/2)\pi] + V_0\}. \tag{5}$$

Here $V_1 = 0.004$, $V_0 = 0.03$ and $L_{cx} = L_x/5$. As seen in expression (5), the waveform perturbation is superimposed on the uniform inflow V_0, and V_z reaches the maximum and minimum at $x/L_{cx} - 5/2 = 0$, ±2 and $x/L_{cx} - 5/2 = \pm1$, respectively.

[11] The 2.5-D MHD equations are solved by a new Hall MHD code [*Yang and Jin*, 2004] derived from multistep implicit scheme [*Hu*, 1989]. In the present simulation, the computational domain is divided into 241×61 grid points. In order to allow adequate spatial resolution in the current sheet, the grid spacing in the z direction from $z = 0$ to $z = \pm L_z$ increases according to a geometric series. In the x direction, the computation from $x = 0$ to $x = L_x = 12$ is advanced by a uniform grid point spacing $\Delta x = 0.05$. To ensure computational accuracy and numerical stability, the time steps Δt are required to satisfy the following Courant condition: $\Delta t \leq \Delta L/V_{\max}$, where ΔL is the minimum grid spacing and $V_{\max}$ is the maximum of the plasma velocity V in the simulation box.

3. Simulation Results

[12] The initial equilibrium state is driven by waveform inflows imposed at the top and bottom boundaries and three reconnection X lines are formed in the long current sheet. In the absence and presence of an initial guide field B_{y0} the

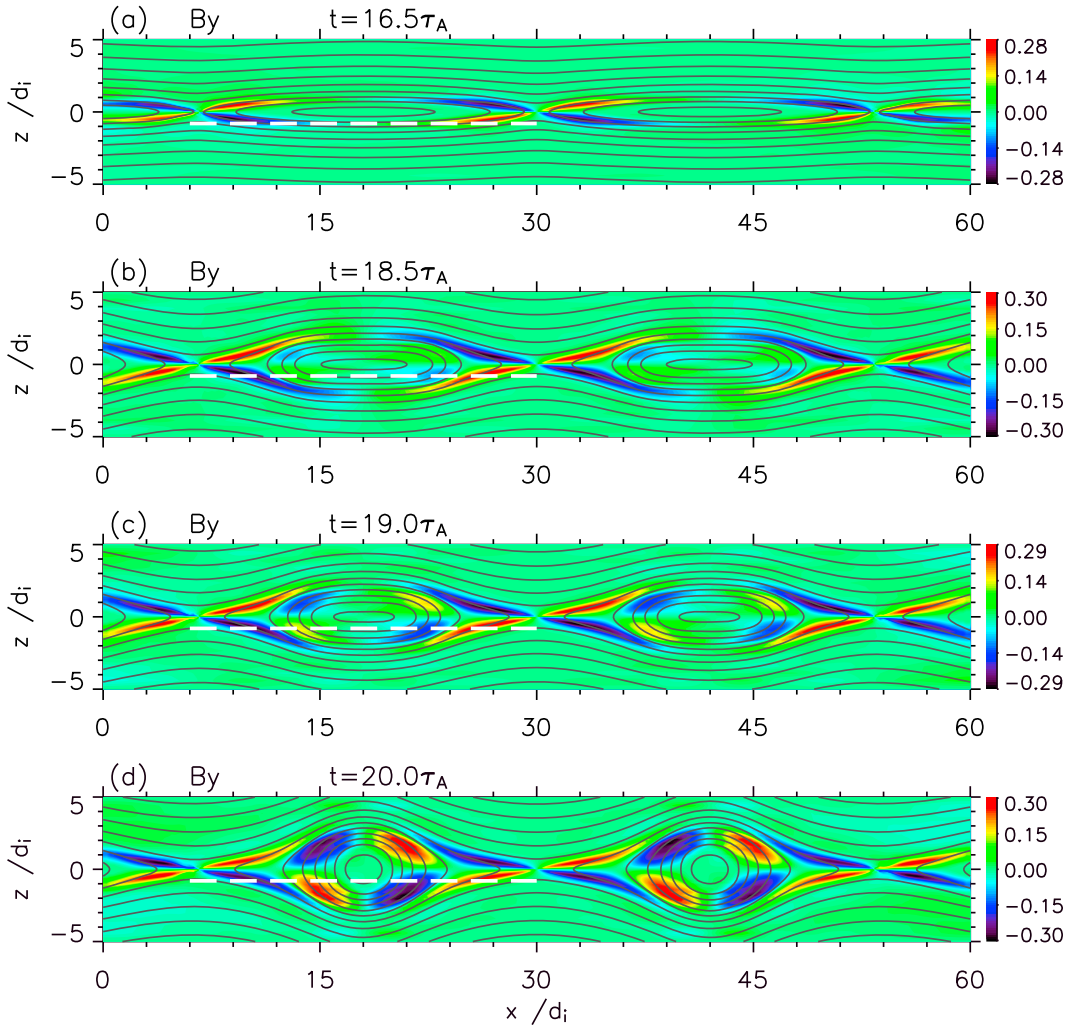

Figure 1. The magnetic field lines (solid lines) and the contours of out-of-plane magnetic field B_y (color plots) for Case 1 with $B_{y0} = 0$ at (a) $t = 16.5\tau_A$, (b) $t = 18.5\tau_A$, (c) $t = 19.0\tau_A$ and (d) $t = 20.0\tau_A$.

behaviors of the plasmoids bound between two neighboring reconnection sites are investigated using a Hall MHD code [*Yang and Jin*, 2004].

3.1. Case 1: $B_{y0} = 0$

[13] The time evolution of Hall MHD reconnection with three X lines is shown in Figure 1 where the magnetic field lines (i.e., the contours of $A(x, z)$) and the contours of the out-of-plane magnetic field B_y are expressed by the solid lines and the color plots, respectively. As seen in Figure 1a ($t = 16.5\tau_A$), two flat plasmoids are bound between two adjacent X lines, and B_y has the expected quadrupole structure at every one of three X lines. The picture of B_y in a plasmoid consists of the quadrupole B_y fields generated by two adjacent X lines. During the evolution phase shown in Figure 1 the size of the plasmoid in the z direction gradually increases and so the opennesses of the quadrupolar B_y structures in the plasmoid are correspondingly extended. Some fine structures of B_y contours with the reversed sign emerge and gradually grow within the original B_y structures, as seen in Figure 1b ($t = 18.5\tau_A$) and Figure 1c ($t = 19\tau_A$). The plasmoids with a rather large extent in the z direction are composed of two distinct regions in Figure 1d ($t = 20\tau_A$): The quadrupolar B_y structures in the outer regions are determined by the neighboring X lines. The inner regions enveloped in the outer regions consist of the new emerging B_y quadrupole structures which have the B_y polarities as opposed to those in the outer regions. The plasma inflow does not transfer any B_y flux to the reconnection region since B_y is kept up the initial magnitude ($B_{y0} = 0$) along the top and bottom boundaries in Case 1. Consequently, the maximum and minimum of B_y are maintained at about ±0.3 in the reconnection process as seen in the color bar of Figure 1, and the generation of the inner B_y structures is independent of external mechanism. The B_y picture including the inner and outer quadrupole structure in Figure 1 is somewhat similar to the intensity plot of out-of-plane field from the hybrid simulation by *Karimabadi et al.* [2004].

[14] The velocity vector plots of the in-plane ion and electron flows at $t = 20\tau_A$ are illustrated in Figures 2a and 2b, respectively. In Hall MHD the ion flow velocity $\mathbf{V}_i \approx \mathbf{V}$ and the electron flow velocity can be expressed as $\mathbf{V}_e \approx \mathbf{V} - K_H\mathbf{J}/n$, where n is the proton density (in a hydrogen

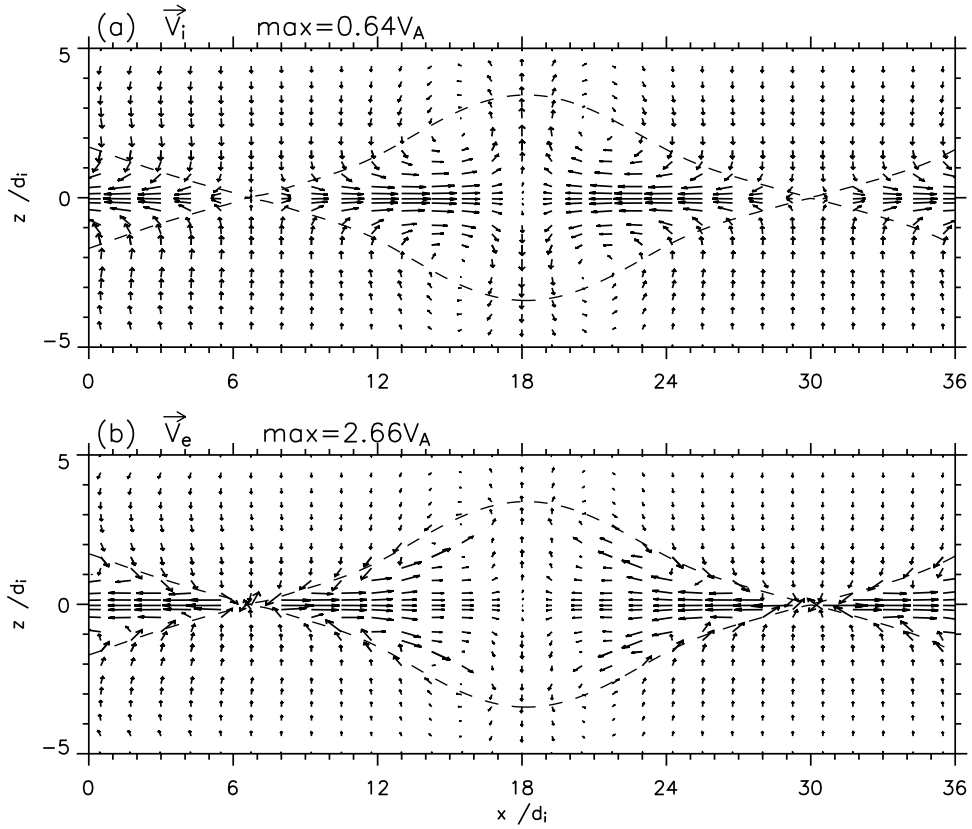

Figure 2. The velocity vector plots of (a) ion flow and (b) electron flow in the (x, z) plane at $t = 20\tau_A$ for Case 1 ($B_{y0} = 0$).

plasma). In order to clearly illustrate the distributions of ion and electron flow in a plasmoid, only the data for $0 \leq x \leq 36d_i$ are used in the Figure 2 plotting. The waveform inflow is imposed at the top and bottom boundaries and the jets are ejected from the X lines in Figure 2. When the flows toward the central part of the plasmoid run into each other, the flow with a positive V_x runs head on to the flow with a negative V_x and then the flows are deflected to the upper and lower sides. The outflows along the z direction are formed in the central region of the plasmoid and result in the extension of the plasmoid in the z direction. As seen in Figures 2a and 2b, the ion flow and electron flow are the symmetric patterns with respect to the x axis ($z = 0$) and the plasmoid center. The maximum speed of the electron flow ($V_e|_{\max} = 2.66V_A$) is much larger than that of ion flow ($V_i|_{\max} = 0.64V_A$). In particular, the electron flow is much faster than the ion flow near the X lines. It indicates that the motion of electrons and ions decouples in the vicinity of the X lines.

[15] In order to get a better understanding of the time evolution in the magnetic signature within the plasmoid, at four different times (t = 16.5, 18.5, 19.0 and $20.0\tau_A$) we have plotted the profiles of the field components B_x (dashed line), B_y (solid line) and B_z (dot-dashed line) along x at $z = -0.8d_i$ in Figure 3 (the cuts are marked by the white dashed lines in Figure 1). The component B_z has the familiar bipolar signature which is first negative and then switches to positive. The amplitude of the B_z bipolar signature enhances and the interval between the bipolarity shortens as the time elapses. The B_x component reaches the maximum at the edges of the plasmoid and becomes of the minimum at the center of plasmoid. The profiles of B_x are the concave curves and the depth of the concave-down signature increases with time, as seen in Figure 3. Note that the profiles in Figure 3 are plotted along the cuts with same location at four separate times and so such developing behaviors in both B_x and B_z are related to the extension of the plasmoid in the z direction. In addition, there is a more notable time evolution in the profiles of the out-of-plane component B_y. At $t = 16.5\tau_A$ the B_y profile is a bipolar signature (−/+) which is associated with the B_y field generated by two neighboring X lines. The amplitude of the bipolar signature with (−/+) patten enhances and a new bipolar signature, which is first positive and switches to negative, appears between the original (−/+) signatures at $t = 18.5\tau_A$. The inner (+/−) bipolar signature, which arises from the new emerging B_y quadrupole structure in the plasmoid, grows with time and its amplitude is almost equal to that in the original bipolar signature at $t = 20\tau_A$. In Case 1 the B_y profiles including inner and outer bipolar variations exhibit a wavelike fluctuation feature that is similar to the hybrid simulation by *Karimabadi et al.* [1999]. The bipolar and wavelike signatures of B_y in Figure 3 are in line with the observed features of a closed-loop plasmoid in the magnetotail. The waveform features in both B_y and B_z were investigated using an MHD simulation without Hall effect [*Jin et al.*, 2001]. Some of multiple plasmoids in the cases of Type II showed the bipolar variations of the B_y component, but such signatures with very small amplitudes was not a good representation of the observed bipolar feature in the B_y component [*Deng et al.*, 2004; *Zong et al.*, 1997;

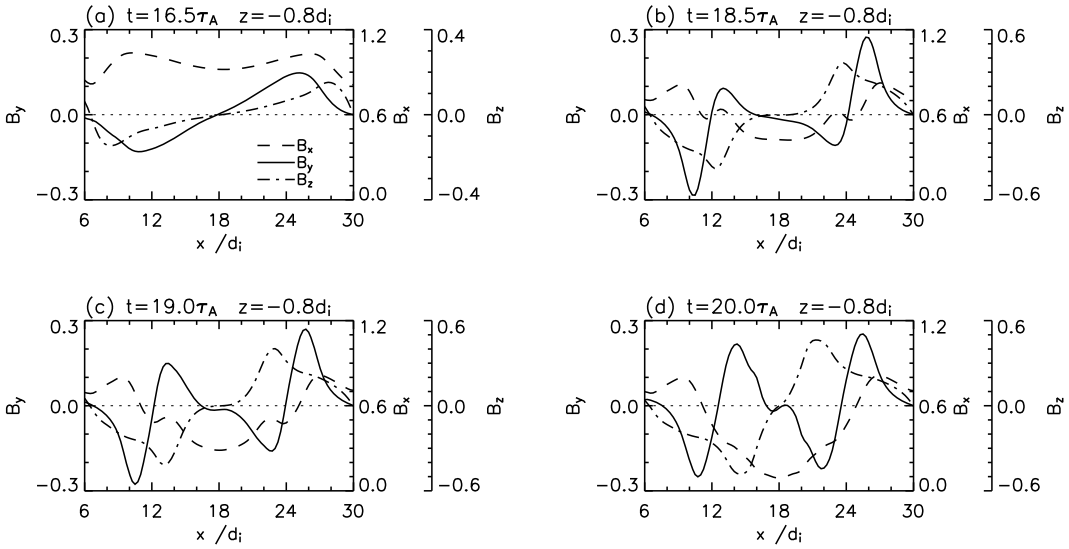

Figure 3. The profiles of three components, B_x (dashed line), B_y (solid line), and B_z (dot-dashed line), of magnetic field along x at $z = -0.8d_i$ for Case 1 with $B_{y0} = 0$ at (a) $t = 16.5\tau_A$, (b) $t = 18.5\tau_A$, (c) $t = 19.0\tau_A$ and (d) $t = 20.0\tau_A$.

Moldwin and Hughes, 1992] due to the absence of Hall effect.

3.2. Case 2: $B_{y0} = 0.1$

[16] At $t = 16.5\tau_A$ and $t = 19.0\tau_A$ the magnetic field configuration and the B_y contours are shown in Figures 4a and 4b, respectively. The reconnection configurations in Figure 4 are similar to those in Figure 1. The pictures of B_y in Case 2 of $B_{y0} = 0.1$ have somewhat resemblance to those in Case 1 ($B_{y0} = 0$). However, due to the addition of $B_{y0} = 0.1$ the maximums and minimums of B_y contours in Case 2 are larger than those in Case 1, as shown in the color bars of Figure 1. At $t = 19.0\tau_A$ the inner B_y structure, in which the red areas with $B_y > 0.1$ are larger than blue areas with $B_y < 0.1$, has formed in the plasmoid. To compare with Case 1, the profiles of the field components B_x (dashed line), B_y (solid line) and B_z (dot-dashed line) along x at $z = -0.8d_i$ at four corresponding times are illustrated in Figure 5. The time evolutions of the B_x and B_z components in Figure 5 resemble to those in Figure 3. Some differences can be found by the comparison between the B_y profiles in Case 2 and Case 1. At $t = 16.5\tau_A$ the B_y profile is a bipolar variation with respect to $B_{y0} = 0.1$, which is first less than 0.1 and then switches to be larger than 0.1. The variation amplitude with $B_y > 0.1$ is obviously larger than that with $B_y < 0.1$ in the B_y signature. A new bipolar variation about $B_y = 0.1$, which is first larger than 0.1 and switches to be less than 0.1, appears between the minimum and maximum associated with the original B_y signature at $t = 18.5\tau_A$. The inner signature associated with the new emerging B_y structure grows with time and a wavelike fluctuation signature of B_y component occurs in Figures 5c and 5d. The fluctuation signatures have an asymmetric feature, namely, its amplitude and width in the $B_y > 0.1$ region are notably larger than those in the $B_y < 0.1$ region in Case 2 with a small guide

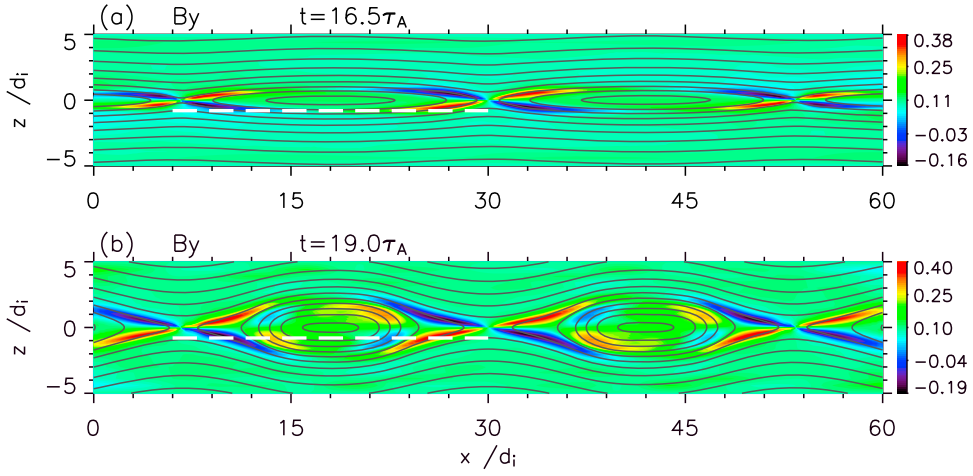

Figure 4. The magnetic field lines (solid lines) and the contours of out-of-plane magnetic field B_y (color plots) for Case 2 with $B_{y0} = 0.1$ at (a) $t = 16.5\tau_A$ and (b) $t = 19.0\tau_A$.

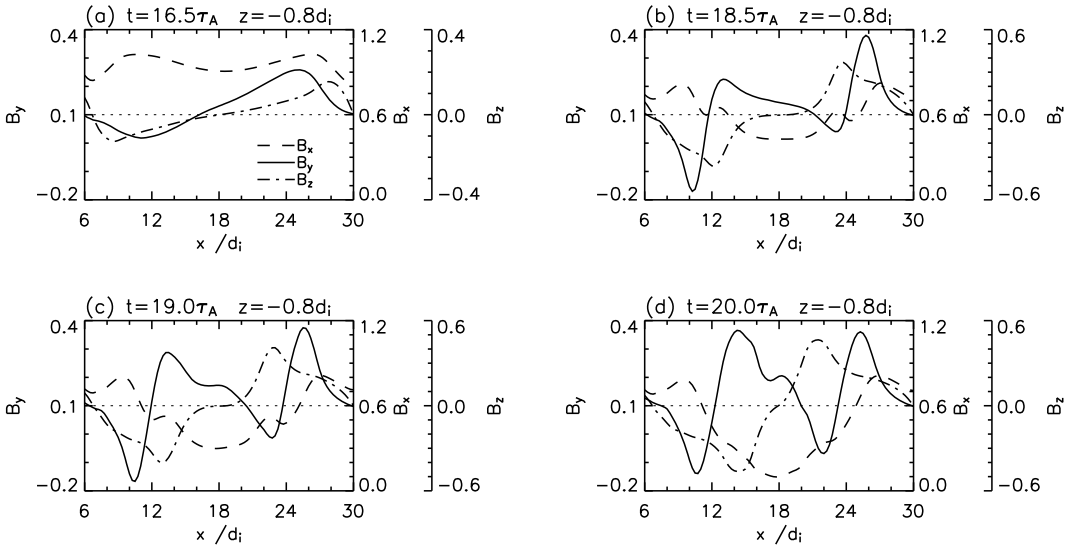

Figure 5. The profiles of three components, B_x (dashed line), B_y (solid line), and B_z (dot-dashed line), of magnetic field along x at $z = -0.8d_i$ for Case 2 with $B_{y0} = 0.1$ at (a) $t = 16.5\tau_A$, (b) $t = 18.5\tau_A$, (c) $t = 19.0\tau_A$, and (d) $t = 20.0\tau_A$.

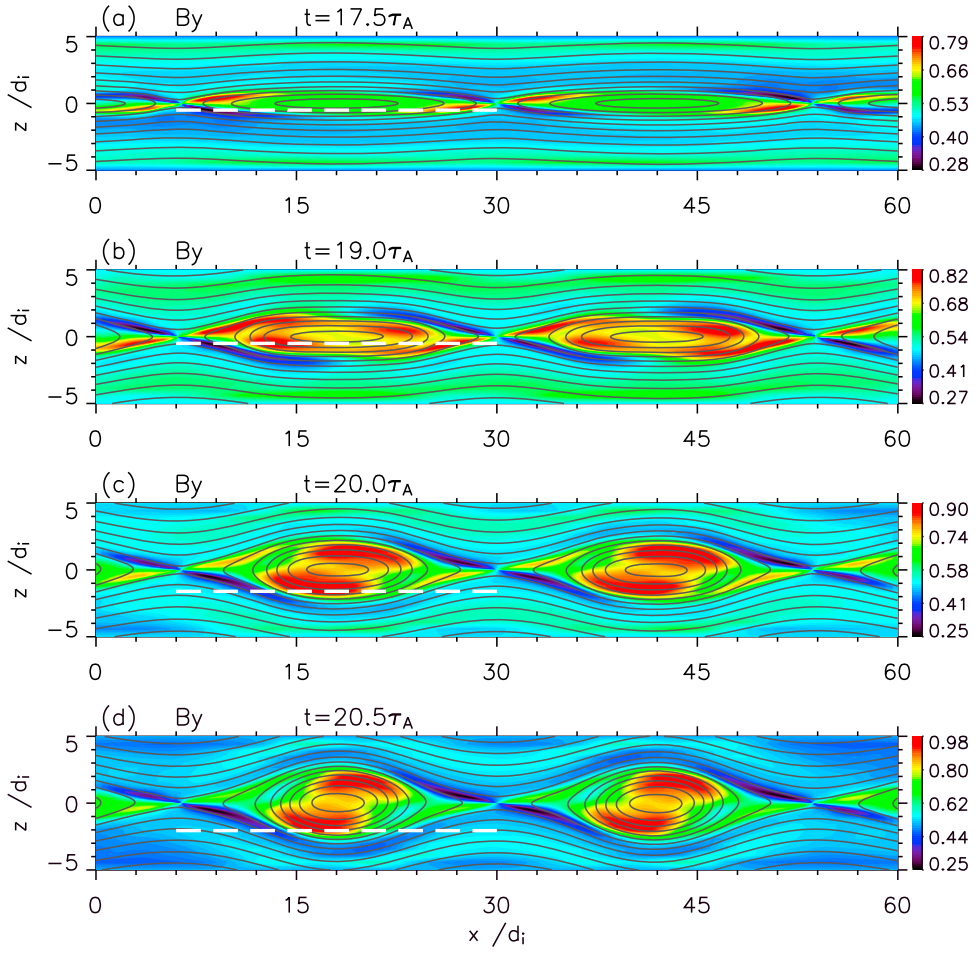

Figure 6. The magnetic field lines (solid lines) and the contours of out-of-plane magnetic field B_y (color plots) for Case 3 with $B_{y0} = 0.5$ at (a) $t = 17.5\tau_A$, (b) $t = 19.0\tau_A$, (c) $t = 20.0\tau_A$, and (d) $t = 20.5\tau_A$.

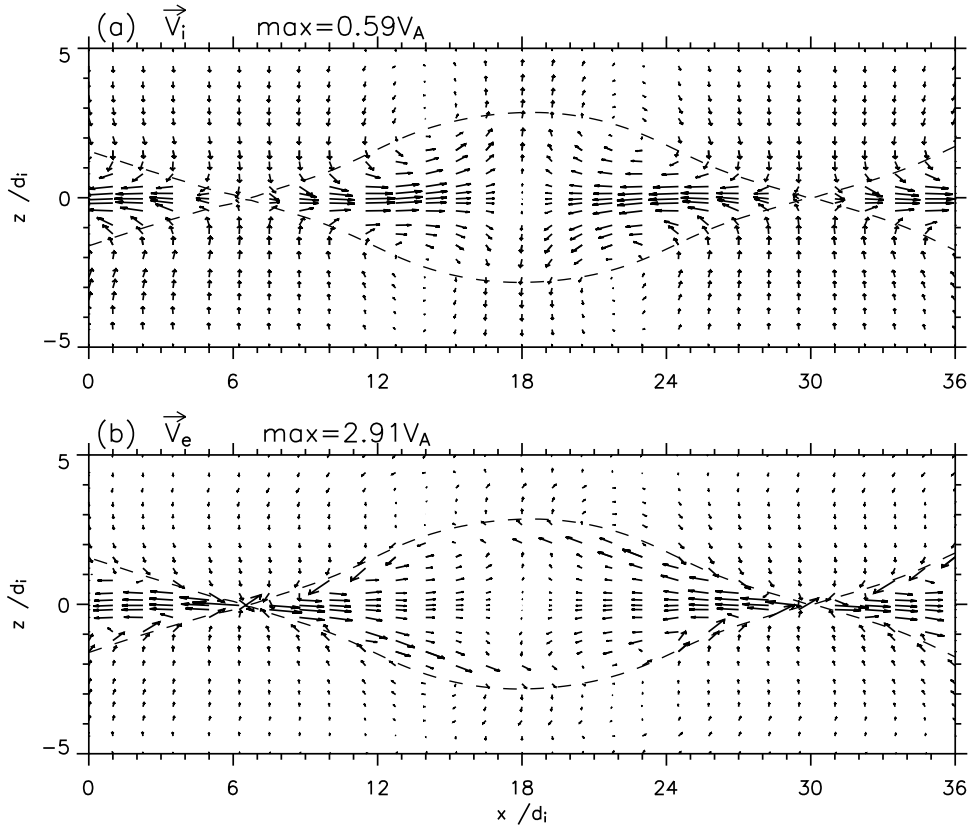

Figure 7. The velocity vector plots of (a) ion flow and (b) electron flow in (x, z) plane at $t = 20\tau_A$ for Case 3 ($B_{y0} = 0.5$).

field ($B_{y0} = 0.1$). The asymmetric behavior of the B_y signature becomes more notable as B_{y0} increases. The B_y profile is translated into a unipolar variation with $B_y > 0$ when B_{y0} reaches or exceeds 0.3.

3.3. Case 3: $B_{y0} = 0.5$

[17] At four separate times (t = 17.5, 19.0, 20.0 and $20.5\tau_A$) the situations of multiple X line reconnection are shown in Figure 6, in which the magnetic field lines and the contours of the out-of-plane magnetic field B_y are marked by the solid lines and the color plots, respectively. The plasmoids are bound between two adjacent X lines and the basic behavior in the magnetic field configuration of Case 3 ($B_{y0} = 0.5$) is similar to that of Case 1 with $B_{y0} = 0$, as seen in Figure 6. However, the plot of B_y in Figure 6 is notably different from that in Figure 1. As seen in Figure 6, the B_y field changes from a quadrupolar to a unipolar structure with positive value at every one of the X lines due to the addition of the initial guide field $B_{y0} = 0.5$. Such a unipolar B_y structure with four branches is referred to as the four-wing structure in the following. The intensity of B_y in the plasmoid is nearly a constant ($B_y \approx 0.55$) until $t = 17.5\tau_A$ as seen in Figure 6a. In this phase ($t \leq 17.5\tau_A$) B_y in the plasmoid gradually increases due to the continuous addition of B_y flux which is carried from the lobe regions near the boundaries into the plasmoid-like regions by the plasma inflows imposed at the top and bottom boundaries where B_y is maintained at its initial value ($B_{y0} = 0.5$). The size of the plasmoid in the z direction gradually increases and the opennesses of the B_y structures are correspondingly extended in Figure 6, which is similar to that in Figure 1. There occur two red regions with enhanced B_y near the four-wing structures at two neighboring X lines in Figure 6b ($t = 19\tau_A$). The enhanced B_y regions in Case 3 resemble to the inner quadrupole B_y structures in Case 1 ($B_{y0} = 0$), but the regions with $B_y < 0.5$ disappear in the new emerging structure at $t = 19\tau_A$ due to the presence of the guide field $B_{y0}(= 0.5)$. The additional B_y flux carried by the plasma flow result in the inward shift of two red regions with enhanced B_y. An S-shaped region is formed within the plasmoids while the two red B_y regions connect each other, as seen in Figures 6c and 6d. The similar result from the hybrid simulation was obtained by *Karimabadi et al.* [1999]. In Figures 6a, 6b, and 6c the B_y pictures have evolved into the nonuniform patterns including the red regions with the enhanced B_y and the green (or blue) regions with the reduced B_y in the plasmoids. The blue and green regions with the reduced B_y extend while the B_y intensity in the red region enhances, as seen in Figures 6c and 6d. This indicates that the B_y field is transferred and concentrated onto the red regions after the occurrence of the enhanced B_y regions caused by Hall effect. As a result the maximum of B_y ($B_y|_{\max}$) in the plasmoid rapidly strengthens. We suggest that the rapid growth of core B_y field in the plasmoid might be associated with the Hall effect since the concentration of B_y field takes place after the emergence of the enhanced B_y regions. However, the concentration of B_y field and the rapid growth of $B_y|_{\max}$ do not occur in Case 1 with Hall effect. This difference in the two cases is related to that there is the continuous addition of B_y flux in Case 3 ($B_{y0} = 0.5$), but there is no such addition in Case 1 ($B_{y0} = 0$). It implies that the rapid growth of $B_y|_{\max}$ in

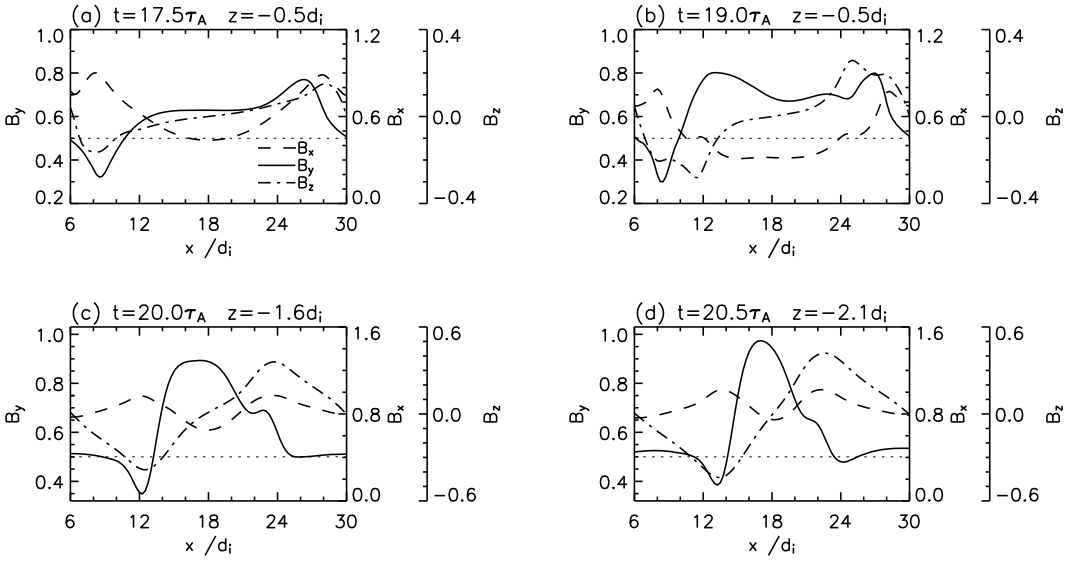

Figure 8. The profiles of three components, B_x (dashed line), B_y (solid line), and B_z (dot-dashed line), of magnetic field for Case 3 with $B_{y0} = 0.5$ at (a) $t = 17.5\tau_A$, (b) $t = 19.0\tau_A$, (c) $t = 20.0\tau_A$, and (d) $t = 20.5\tau_A$ along the cuts which are marked by the white dashed lines in Figure 6.

the plasmoid in the later phase might be attributed to the interaction between Hall effect and the additional B_y flux in Case 3. A further discussion on the growth of core field can be found in section 4.

[18] The velocity vector plots of the in-plane ion and electron flows at $t = 20.0\tau_A$ are illustrated in Figures 7a and 7b, respectively. The maximum speed of the electron flow ($V_e|_{\max} = 2.91V_A$) is much larger than that of ion flow ($V_i|_{\max} = 0.59V_A$) and so there is the decoupling of electron and ion in vicinity of the X line in Case 3 as well. As seen in Figure 7, the ion flow remains approximately symmetric with respect to the x axis ($z = 0$), but the electron flow becomes an asymmetric pattern. Near the edge of the plasmoid the electrons have a stronger flow pointing to the central region of plasmoid in the upper right and lower left quadrants, whereas they have a flow pointing to the X line in the upper left and lower right quadrants of the plasmoid. The initial magnetic field is a noncoplanar field due to the presence of guide field $B_{y0}(= 0.5)$ in Case 3. It can be found by comparing Figure 7 with Figure 2 that the outflow along the z direction in Case 3 is weaker than that in Case 1. Such a weaker flow in the z direction is attributed to a less deflection of the flow in the noncoplanar Case 3 where the plasma flows with positive and negative V_x are displaced with respect to each other, as the situation interpreted by *Karimabadi et al.* [1999]. As a consequence the extension of plasmoid in the z direction in Case 3 is slower than that in Case 1. This feature is comparable to that in Hall MHD reconnection with a single X line [*Yang et al.*, 2008] in which the openness of the magnetic separatrix angle is slightly reduced as a nonzero B_{y0} is added.

[19] Figure 8 shows the profiles of the field components B_x (dashed line), B_y (solid line) and B_z (dot-dashed line) along the cuts which are set on the different locations at $t =$ 19.0, 20.0 and $20.5\tau_A$ (the cuts are marked by the white dashed lines in Figure 6). The component B_z in Figure 8 is a well-known bipolar signature with −/+ pattern and the amplitude of the bipolar signature enhances with time. The field component B_x reaches the maximum at the edges of the plasmoid and becomes of the minimum at the center of the plasmoid and so the B_x profiles also are the concave curves. However, the depth of the concave-down signature in the B_x profile, which is made on the different location at the different time in Figure 8, does not have a regular development like that in Figure 3. It is worthy of note that the B_y profiles of Case 3 display the distinct behavior from Case 1. At $t = 17.5\tau_A$ (Figure 8a) the B_y shows a valley and peak at $x = 8.4d_i$ and $26.3d_i$, which are associated with the B_y four-wing structures at neighboring two X lines. The intensity of B_y between the valley and peak is an approximate constant ($B_y \approx 0.6$). In the early phase ($t \leq 17.5\tau_A$) the approximately uniform B_y in the B_y profiles gradually increases with time due to the inward transportation of the B_y flux from the lobe region near the boundaries. There occurs a B_y bulge associated with the red enhanced B_y region in Figure 8b ($t = 19\tau_A$). The B_y bulge resembles to inner bipolar signature caused by Hall effect in Figure 3b, but the fluctuation with $B_y < 0.5$ disappears in the inner region of the B_y profile due to the presence of the guide field $B_{y0} = 0.5$. The B_y bulge grows into a peaking signature while the B_y flux is transferred and concentrated onto the enhanced B_y regions in the plasmoid. As seen in Figures 8b, 8c, and 8d, the maximum in the B_y peaking signature enhances and the peak's location shifts toward the center of plasmoid as the reconnection proceeds. At $t = 20.5\tau_A$ the maximum of B_y near the center of plasmoid approaches the lobe magnetic field strength. Such a substantial enhancement of the out-of-plane component B_y in the central region of plasmoid might be representative of the observed strong core field in the flux rope structure.

4. Summary and Discussion

[20] The plasmoids have been observed by many spacecrafts in the magnetotail. A large number of plasmoids exhibit a strong core field and were called "magnetic flux

rope," and there also exist the plasmoids with closed-looped magnetic field lines in the magnetotail. As mentioned above, the numerical results in the cases with various guide field B_{y0} exhibit the features of the different plasmoid-like structures. The origination and evolution of the different features will be discussed in what follows.

4.1. Bipolar and Wavelike Signature of B_y in Case 1 ($B_{y0} = 0$)

[21] As seen in Figure 1, the picture of B_y in a plasmoid consists of the quadrupole B_y fields generated by two adjacent X lines in the early phase, and then it evolves into two regions with different quadrupole structures. The inner region is composed of the new emerging B_y having the opposite polarities from those in the outer region. The profile of B_y component correspondingly develops from a bipolar signature into a bipolar fluctuation signature. There is no addition of B_y flux since B_y is maintained at zero along the top and bottom boundaries; in other words, the formation of the bipolar and fluctuation signatures is independent of the external mechanism in Case 1 with $B_{y0} = 0$. As seen in Figure 2, the outflows along the z direction are formed in the central region of the plasmoid and result in the extension of the plasmoid in the z direction. The new B_y structures emerge within the original quadrupole structure when its openness is extended to large enough. This situation is rather similar to our previous result [*Jin et al.*, 2005] in which the openness of the quadrupolar B_y structure is enlarged as β increases and the fine structures of B_y contours with the reversed signs emerge as $\beta > 2.0$.

[22] In order to get a better understanding of the inner B_y structures, at four separate times we have plotted the profiles of both x and z components in the electron velocity V_e and ion velocity V_i as well as the profiles of B_y component at $z = -0.8d_i$ along x in Figure 9 where V_e and V_i are marked by the solid line and dashed line, respectively. In Figure 9 the profiles of V_{ix}, V_{ex} (first plot) and the profiles of V_{iz}, V_{ez} (second plot) display the time evolution of the decoupling motion between the electrons and ions: At $t = 16.5\tau_A$ the V_{ix} signature with a small amplitude is first positive and then switches to negative, but V_{ex} switches from negative to positive via a central range with zero magnitude, and so there exists the obvious separation of V_{ex} and V_{ix} in two regions of the profiles. In the second plot of Figure 9a V_{ez} only slightly separates from V_{iz}. The profile of B_y in Figure 9a is a bipolar signature associated with the B_y quadrupolar structures at two neighboring X lines. It can be found comparing the B_y profile with the profiles of V_{ex} and V_{ix} that the B_y bipolar signature is corresponding to the decoupling regions of electrons and ions in Figure 9a. At $t = 18.5\tau_A$ the amplitude in the (+/−) bipolar signature of V_{ix} is notably larger than that at $t = 16.5\tau_A$. The original (−/+) bipolar signature of V_{ex} becomes narrower and a new V_{ex} bipolar signature with (+/−) pattern occurs inside the original (−/+) signature in first plot of Figure 9b. In second plot of Figure 9b the profile of V_{iz} still is a concave curve, but V_{ez} shows the bipolar variations with +/− and −/+ patterns at the left and right sides of the plasmoid. A new bipolar B_y signature with (+/−) pattern appears inside the original (−/+) B_y signature in third plot of Figure 9b. Interestingly, the new bipolar B_y signature coincides with the regions where later decoupling of the electrons and ions takes place. As seen in Figure 9c ($t = 19.0\tau_A$) and Figure 9d ($t = 20.0\tau_A$), the inner B_y bipolar signature grows up as the separation between V_{ex}, V_{ez} and V_{ix}, V_{iz} develops. Therefore, the reversal currents caused by the additional decoupling of electrons and ions might be responsible for the inner bipolar signature corresponding to the inner quadrupole structure of B_y in Figure 1; in other words, the observed bipolar or waveform signature of B_y component in the closed-loop-like plasmoid might arise from the effect of Hall current. As mentioned in Case 2, the bipolar feature still exists in the B_y profile although the variation amplitude with $B_y > 0$ is considerably larger than that with $B_y < 0$ in the presence of a small guide field ($B_{y0} = 0.1$) and the asymmetric behavior becomes more notable as B_{y0} increases. Such an asymmetric bipolar feature of B_y component could be comparable with a closed-loop plasmoid. The typical feature of a magnetic flux rope is shown in the cases with $B_{y0} \geq 0.3$. The result in Case 2 with $B_{y0} = 0.1$ might exhibit the transition situation from the closed-loop plasmoid to magnetic flux rope.

4.2. Development of the Core Field Within the Plasmoid for the Cases With $B_{y0} \geq 0.3$

[23] When B_{y0} reaches or exceeds 0.3, the B_y component is the positive everywhere, which is in line with the hybrid simulation by *Karimabadi et al.* [1999] and the Hall MHD simulations with a single X line by *Yang et al.* [2008] and *Huba* [2005], and the B_y profile becomes of a unipolar variation. As shown in Case 3 ($B_{y0} = 0.5$), a B_y bulge appears as the enhanced B_y regions take place in the plasmoid, and then it grows into a peaking signature in the B_y profile of Figure 8. The maximum in the B_y peaking signature increases with time and approaches the lobe magnetic field strength. Such a substantial enhancement of the out-of-plane component B_y in the central region of plasmoid is consistent with the observed feature of strong core field in the flux rope structure.

[24] In order to get a better understanding of the growth of the core field, we investigate the cases with $B_{y0} \geq 0.3$. Figure 10 shows the time history of the B_y component at the center of the plasmoid ($x = 18d_i$, $z = 0d_i$), which is referred to as B_y* in the following, for five cases with $B_{y0} = 0$, 0.3, 0.5, 0.7 and 1.0. As seen in Figure 10, the evolution of B_y* can be divided into two stages: At the first stage the intensity of B_y* gradually increases with time, while the B_y component is approximately uniform in the plasmoid. The gradual enhancement of B_y in the plasmoid is attributed to the continuous addition of B_y flux from the lobe regions near the top and bottom boundaries where B_y is maintained at its initial value $B_{y0} = 0.5$. In the first phase the mean increasing rates of B_y*, $\Delta B/\Delta t$ increases with increasing B_{y0}, namely, the growth of B_y* becomes faster as B_{y0} increases. In addition, the B_y* remains zero throughout the reconnection process in Case 1 ($B_{y0} = 0$). The reason is that there is no the addition of B_y flux since the B_y component at the top and bottom boundaries is maintained at zero in Case 1. Interestingly, for four cases with a finite B_{y0} in Figure 10 the intensity of B_y* is quickly raised at the second stage that starts from the occurrence of the enhanced B_y region in the plasmoid. The enhanced B_y regions resembling to the inner quadrupole B_y structures in Case 1, are also generated by Hall current associated with the

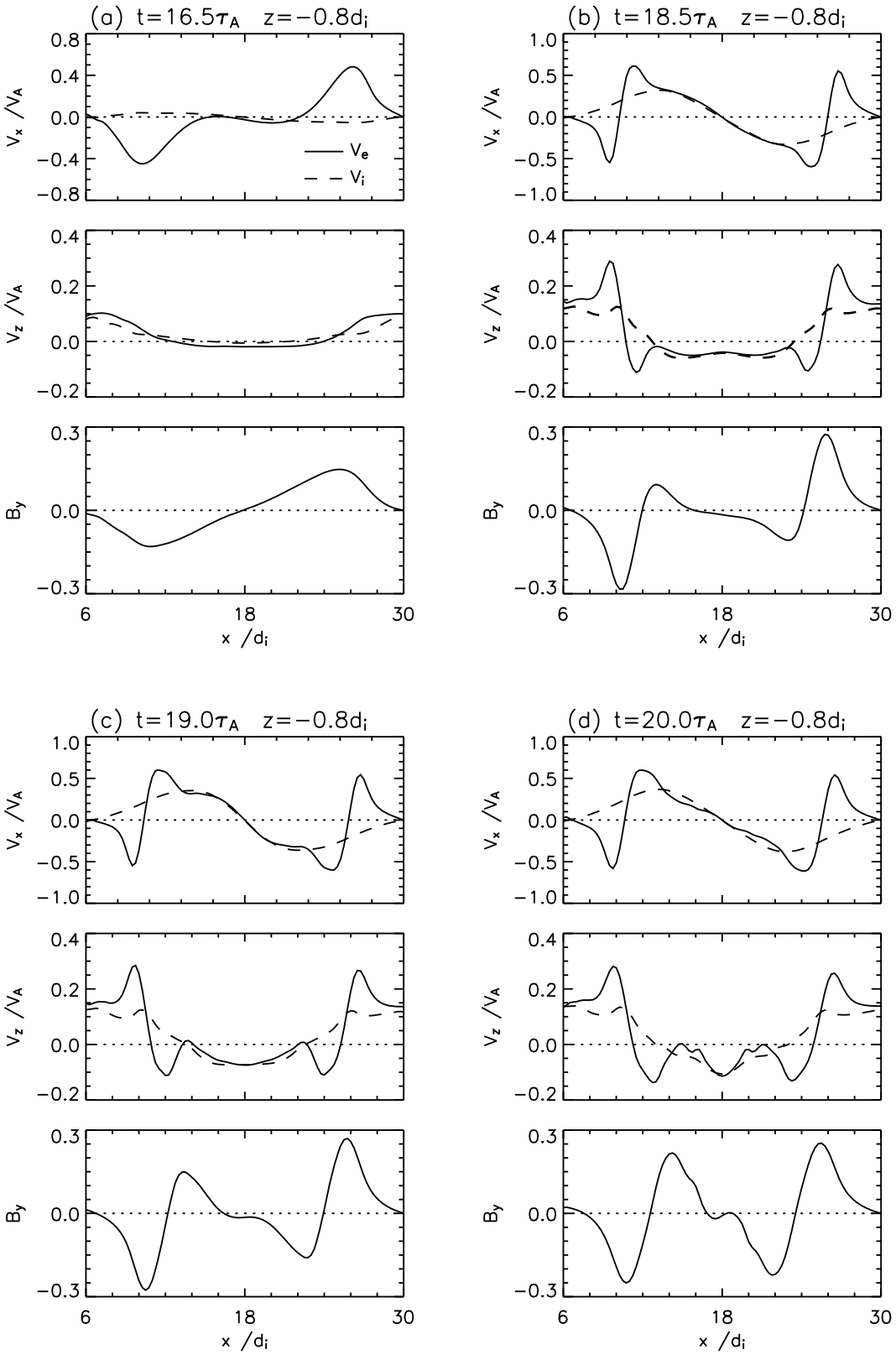

Figure 9. The profiles of both x and z components in the electron velocity V_e (solid line) and ion velocity V_i (dashed line), and the profiles of the B_y component along x at $z = -0.8d_i$ for Case 1 with $B_{y0} = 0$ at (a) $t = 16.5\tau_A$, (b) $t = 18.5\tau_A$, (c) $t = 19\tau_A$, and (d) $t = 20\tau_A$.

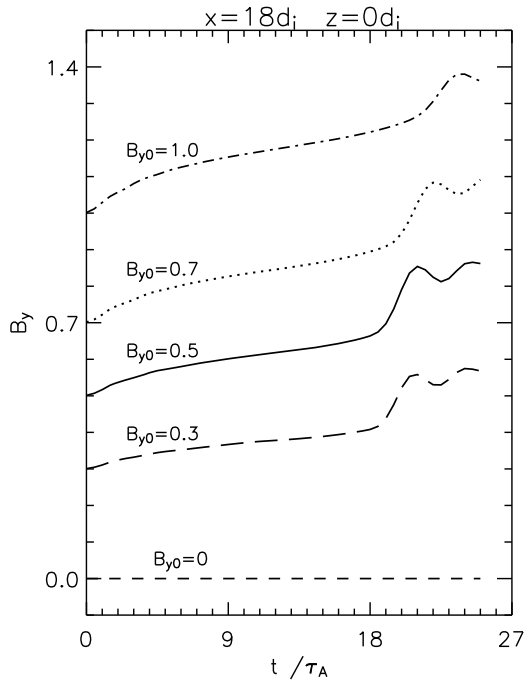

Figure 10. Time history of the B_y component (i.e., B_y*) at the center ($x = 18d_i$, $z = 0d_i$) of the plasmoid for five cases with $B_{y0} = 0$, 0.3, 0.5, 0.7, and 1.0.

decoupling of electrons and ions. As is readily evident from Figure 10, the nonlinear development in the second phase can make a greater contribution than the simple superposition of the B_y flux added by the plasma inflow to the growth of the core B_y field in the cases with $B_{y0} \geq 0.3$. In the second phase an S-shaped region is formed, the B_y field is concentrated onto the enhanced B_y region and the maximum of B_y rapidly strengthens while the B_y is continuously translated into the plasmoid-like regions, as shown in Case 3 ($B_{y0} = 0.5$). In contrast, the enhancement of B_y* does not occur although there also exists the Hall effect in Case 1 ($B_{y0} = 0$). The reason might be that there is no the continuous addition of B_y flux in Case 1. This implies that the nonlinear enhancement of the core B_y field might arise from the interaction between the Hall effect and the continuous addition of B_y flux. In the second phase B_y* is the enhanced B_y intensity and its time evolution is representative of rapid growth of B_y intensity in the enhanced B_y region, but B_y* does not necessarily be the maximum of B_y ($B_y|_{\max}$, i.e., the intensity of the core field) and the location of $B_y|_{\max}$ varies with time in the second stage. In order to illustrate the differences between B_y* and $B_y|_{\max}$, we have plotted $B_y|_{\max}$ and B_y* at $t = 20\tau_A$ as a function of B_{y0} in Figure 11. As seen in Figure 11, $B_y|_{\max}$ and B_y* are almost linearly raised, and B_y* gradually approaches $B_y|_{\max}$ as B_{y0} increases; in other words, the larger the initial guide field B_{y0} is, the stronger the intensity of the core field is and the closer to the center of the plasmoid the core field is.

[25] The results mentioned above indicate that the strong core B_y field in the plasmoid can be created in the presence of a sufficiently large guide field ($B_{y0} \geq 0.3$) and has the same direction as the initial guide field (preexisting cross-tail field). In order to understand the physics of the second stage, the profiles of B_y component at $z = -0.02d_i$ and $z = -0.37d_i$ for Case 3 ($B_{y0} = 0.5$) and Case 1 ($B_{y0} = 0$) are plotted in Figures 12a and 12b, respectively. As seen in Figure 12a, the B_y profiles in the plasmoid at $t = 14.0$, 15.5 and $16.5\tau_A$ are approximate to the level lines. It indicates that there is a region with an approximately uniform B_y in the plasmoid and the intensity of B_y gradually increases with time due to the inward transportation of the B_y flux from the lobe region at the early stage. At $t = 18.0\tau_A$ two B_y bulges associated with the enhanced B_y regions in the plasmoid emerge in the B_y profile. The bulges of B_y grow while they move inward, and coalesce into a peaking signature at $t = 20\tau_A$. The maximum in the B_y peaking signature enhances with time. Such development of the B_y profile corresponding to the second phase in Figure 10, starts from the occurrence of the enhanced B_y region in the plasmoid. There are the following evolving features in the B_y profiles of Figure 12a for $t > 18\tau_A$: (1) The increase in the B_y intensity is accompanied by the contraction of the region with the enhanced B_y. (2) The region with $B_y < 0.6$ extends while B_y in the region with $B_y > 0.6$ rises in Figure 12a, namely, the blue and green regions with the reducing B_y extend while the B_y intensity in the red region enhances, as seen in Figures 6c and 6d. It indicates that the transference and concentration of B_y flux from the region with lower B_y intensity to the red region. In Case 3 there is the continuous addition of B_y flux which is carried from the lobe region into the plasmoid-like regions by the plasma inflows imposed at the top and bottom boundaries where B_y is maintained at its initial value ($B_{y0} = 0.5$). The additional B_y flux might result in the coalescence and compression of the enhanced B_y region. The transference and concentration of B_y flux toward the red regions with the enhanced B_y lead to the rapid rise of the B_y peaking signature in the second phase. In contrast to Figure 12a, the inner bipolar signature of B_y component grows as the decoupling motion between the electrons and ions develops in Figure 12b. However, the inward shift and coalescence of positive and negative signatures do not take place; and there does not exist the transference and concentration of B_y flux in the inner bipolar signature of Case 1. The distinction of Figure 12b from Figure 12a arises from that there is no any addition of B_y flux since B_y is maintained at zero along the top and bottom boundaries in Case 1. These results imply that the interaction between Hall effect and the B_y flux added by the

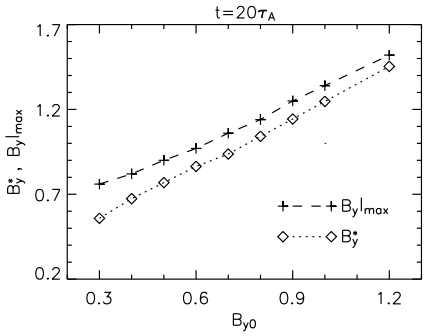

Figure 11. At $t = 20\tau_A$, B_y* and the maximum (i.e., $B_y|_{\max}$) of the B_y component as a function of B_{y0}.

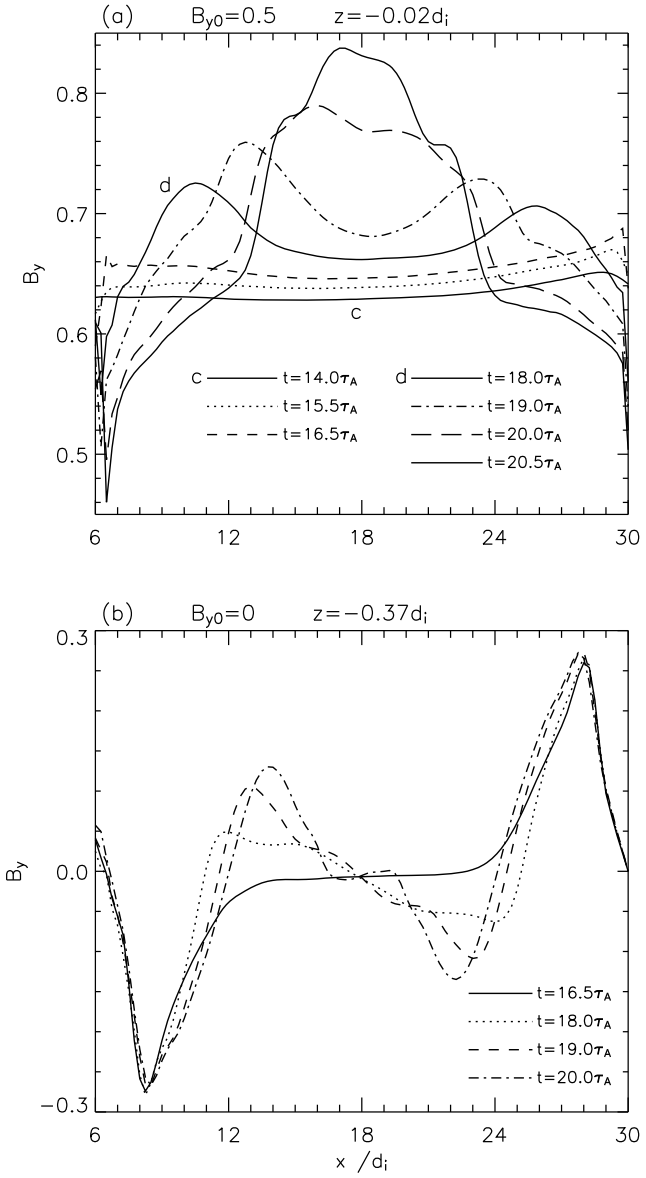

Figure 12. The profiles of the B_y component along x (a) at $z = -0.02d_i$ at seven different times for Case 3 ($B_{y0} = 0.5$) and (b) at $z = -0.37d_i$ at four different times for Case 1 ($B_{y0} = 0$).

plasma inflow might be responsible for the rapid growth of the core B_y field in the second phase of the cases with a finite B_{y0} in Figure 10. Besides, as seen in the time histories of B_y* of Figure 10, B_y* decays and increases once more after it quickly grows to the maximum. Such a process is associated with the temporary extension and succedent contraction of the red enhanced B_y region in the plasmoid.

[26] As mentioned in section 2, the generalized Ohm's law including the Hall current and scalar electron pressure gradient terms is combined in Faraday's induction equation and the 2.5-D Hall MHD equations in dimensionless forms are formed [*Jin et al.*, 2005; *Yang et al.*, 2006]. In the Hall MHD equations the dimensionless parameters χ_m, K_H and K_P are given by the expression (4) and the terms with K_H and K_P are attributed to the effects of the Hall current and pressure gradient in the generalized Ohm's law. In order to investigate the important factor controlling the occurrence and development of the second stage, we take $L_z = L_0 = 7d_i$ and $L_x = 12L_0 = 84d_i$ and carry out the supplementary cases with $B_{y0} = 0.3$, 0.5 and 0.7. Obviously, $K_H = d_i/L_0 = 1/7$ in these cases is smaller than that ($K_H = 1/5$) in the cases of Figure 10. The waveform inflows V_z imposed at the top and bottom boundaries is given by the expression (5). The initial equilibrium state is driven by the waveform inflows, and three reconnection X lines and the plasmoids bound between two adjacent X lines are formed in the simulation box of $L_x/L_z = 12$. In the supplementary case with $B_{y0} = 0.5$ ($L_0 = 7d_i$) the basic behavior of the magnetic field configuration is similar to that in Case 3 ($B_{y0} = 0.5$, $L_0 = 5d_i$), however, the emergence of the red regions with enhanced B_y in the plasmoids is notably postponed in comparison with Case 3. For the further comparison of the cases with $L_0 = 7d_i$ with the corresponding cases ($L_0 = 5d_i$) in Figure 10 the histories of B_y* (i.e., the B_y intensity at the center of the plasmoid) are plotted in Figure 13, in which d_i/V_A is used as the unit of time and the histories of B_y* for the cases of $L_0 = 7d_i$ and $L_0 = 5d_i$ are marked by the dot-dashed lines and the solid lines, respectively. There are also two developing stages in the B_y* histories marked by the dot-dashed lines, as seen in Figure 13. However, the beginning times of the second stage are substantially postponed and the rapid increasing amplitudes of B_y* in the cases with $L_0 = 7d_i$ are obviously smaller than those in the original cases ($L_0 = 5d_i$). The 2.5-D Hall MHD equations in dimensionless forms are numerically solved in the simulation boxes with same dimensionless length ($L_z = 1.0$ and $L_x = 12.0$ in unit of L_0) and the same inflow and

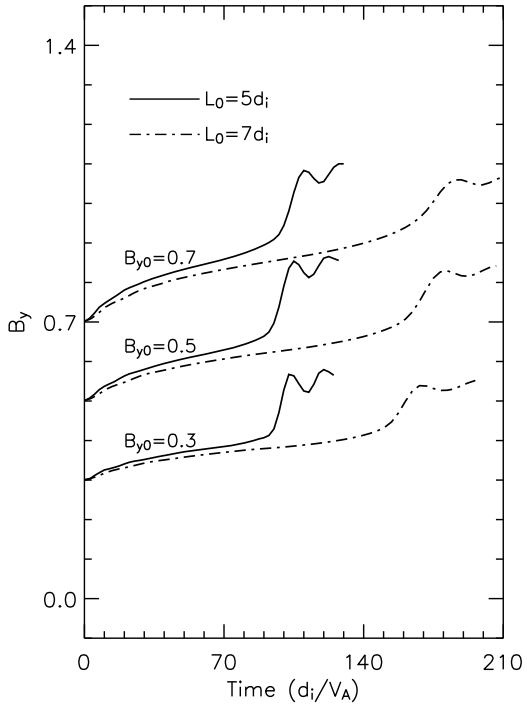

Figure 13. Time history of B_y* (the B_y intensity at the center of the plasmoid) for the cases with $L_0 = 7d_i$ (dot-dashed lines) and $L_0 = 5d_i$ (solid lines) using d_i/V_A as the time unit.

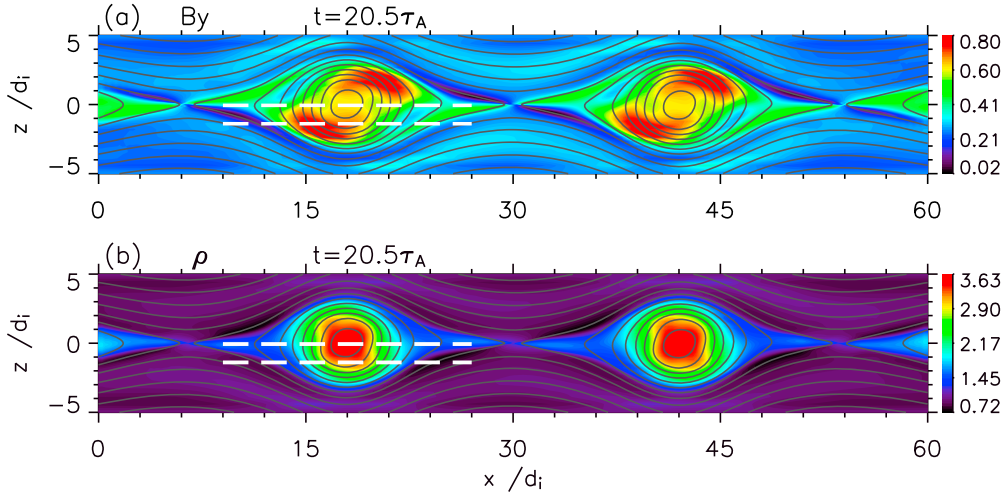

Figure 14. (a) The magnetic field lines (solid lines) and the contours of out-of-plane magnetic field B_y (color plot) and (b) the contours of plasma density (color plot) for Case 4 with $B_{y0} = 0.3$ at $t = 20.5\tau_A$.

boundary conditions are employed in the two types of cases with $L_0 = 7d_i$ and $L_0 = 5d_i$. So in Figure 13 the different features between the B_y* histories marked by the dot-dashed lines and the solid lines are not "the boundary effect," but they are related to the variations of χ_m, K_H and K_P with the different L_0. Moreover, the reconnection behaviors are insensitive to the variations of the resistivity in the cases with the stronger Hall effects [*Yang and Jin*, 2004], and the comparative tests indicate that the reconnection dynamics is controlled by the Hall current effect and the scalar electron pressure gradient is negligible in the cases with the initial guide field $B_{y0} < 1.0$. This means that in the B_y* histories marked by the dot-dashed lines the depression of the B_y* rising amplitudes and the beginning postponement of the second stage are attributed to the reducing Hall effect in the cases with $L_0 = 7d_i$. In consequence, Figure 13 reveals that the intensity of Hall effect has an influence over the generation and evolution of the second phase and it further demonstrates that the interaction between Hall effect and the additional B_y flux is responsible for the rapid growth of the core B_y field in the second phase.

[27] *Chen et al.* [2007] reported the features of the observed islands, such as density compression, bipolar B_z and single-peaked and double-peaked B_y, and demonstrated that these features were the generic signatures of two-dimensional magnetic islands using a Hall MHD simulation with an initial guide field $B_{y0} = 1.0$ [*Chen et al.*, 2007]. The region with a compressed plasma density is consistent with the accumulational region of electrons in the Hall MHD model based on the assumption of the electrical neutrality. In this section we investigate Case 4 with $B_{y0} = 0.3$, which might be comparable in magnitude to a preexisting cross-tail component in the magnetotail. The plots of B_y component and plasma density at $t = 20.5\tau_A$ for Case 4 are shown in Figures 14a and 14b, respectively. As seen in Figure 14, there are a compressed density area and an S-shaped region with the enhanced B_y in the plasmoids, but the S-shaped region does not coincide with the central area with the compressed plasma density in Case 4 ($B_{y0} = 0.3$). It can be found from Figure 11 that the difference between $B_y|_{\max}$ and B_y* decreases with increasing B_{y0}; in other words, the enhanced B_y region gradually approaches the central area of the plasmoid as B_{y0} increases. To compare with the observation we have plotted the profiles of the B_y components (solid line), B_z component (dotted line) and plasma density ρ (dashed line) along cut 1 and cut 2 in Figures 14a and 14b, respectively. Cut 1 at $z = -1.39d_i$ goes across the maximum of B_y and cut 2 at $z = -0.06d_i$ crosses over the central region of the plasmoid. The snapshot of cut 1 (Figure 15a) shows a bipolar B_z pulse, a compressed density region ($\rho_{\max} \sim 3.3$) peaked at the center of the plasmoid, a major peak of ($B_y|_{\max} \sim 0.8$) near the plasmoid's center and a secondary B_y peak related to the four-wing structure of B_y at the X line. Figure 15b illustrates a bipolar B_z, a high density region ($\rho_{\max} \sim 3.6$) and a double peaked B_y in the central region of the plasmoid. The results illustrated in Figure 15a and Figure 15b qualitatively resemble to Cluster observation [*Chen et al.*, 2007], that might be an evidence for the development of core B_y field in the case with a small initial guide field. In order to get a better understanding for the development of compressed plasma density in the plasmoid. At four different times the profiles of plasma density ρ along x at $z = -0.32d_i$ for Case 1 ($B_{y0} = 0$) and Case 4 ($B_{y0} = 0.3$) are shown in Figures 16a and 16b, respectively. In the plasmoid there is a high density region arising from that the current layer is a region with enhanced plasma density in the initial equilibrium state, as seen in Figures 16a and 16b. This region is compressed and the density in the compressed region increases with time. The similar feature in Figure 16a and Figure 16b might be related to the same inflow from the boundaries where ρ is maintained at the initial value ρ_0. The plasma flows from the boundaries and the two X lines compress the regions with higher densities and pile up the plasma within the plasmoids causing the plasma density to be enhanced. This means that the plasma inflow might play an important role in generating the link between compressed plasma density and magnetic islands during reconnection. It can be found by comparing Figure 16b with Figure 16a that the maximums of density $\rho_{\max}$ in Case 4 ($B_{y0} = 0.3$) are about the same as

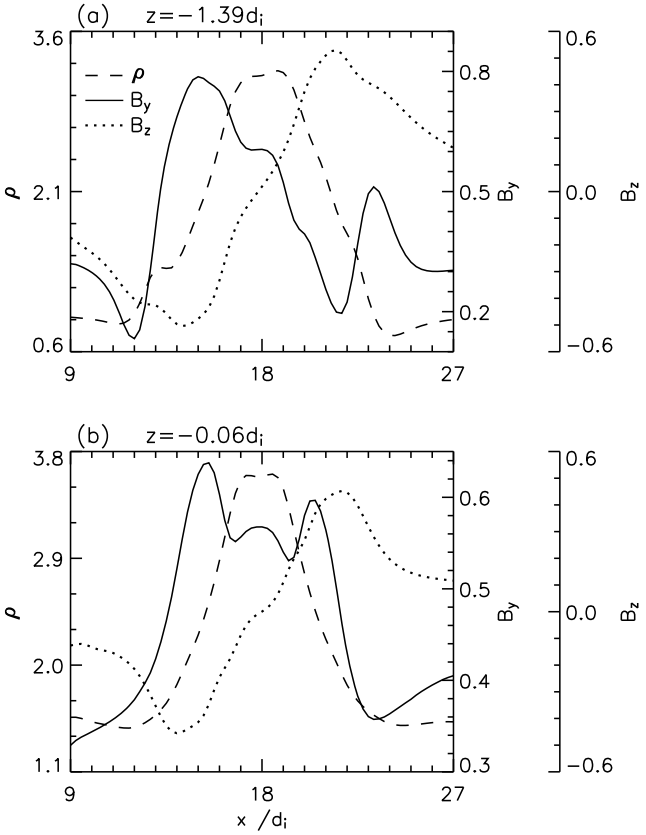

Figure 15. The profiles of the B_y component (solid line), B_z component (dotted line), and plasma density ρ (dashed line) for Case 4 with $B_{y0} = 0.3$ at $t = 20.5\tau_A$ along the two cuts which are marked by the white dashed lines in Figure 14.

those in Case 1 ($B_{y0} = 0$) at $t = 15\tau_A$ and $17\tau_A$. However, $\rho_{max} \approx 2.9$ and $\rho_{max} \approx 3.5$ in Case 4 are lower than $\rho_{max} \approx 3.2$ and $\rho_{max} \approx 3.8$ in Case 1 at $t = 19\tau_A$ and $20\tau_A$, respectively, when B_y* in Case 4($B_{y0} = 0.3$) is rapidly growing, as seen in Figure 10. And ρ_{max} decreases with increasing B_{y0} in a series of cases with various B_{y0} at a corresponding time of the second phase shown in Figure 10. Such results indicate that the compression of plasma density could be restricted due to the growth of core B_y field. Besides, as shown in Figure 16b, the central region of the plasmoid is a compressed density area and also a higher plasma pressure region in Case 4 with $B_{y0} = 0.3$. Therefore, the plasmoid-like structure with a core B_y field in the cases with $B_{y0} \geq 0.3$ could not be characterized as a force-free rope structure.

[28] To conclude, the major results are summarized as follows: (1) The observed features of a closed-loop plasmoid in the magnetotail can be reproduced in the Case 1 with $B_{y0} = 0$. The bipolar and wavelike signatures of B_y component are caused by Hall effect and independent of the external mechanism. (2) The bipolar and fluctuation signatures of B_y have an asymmetric feature with respect to B_{y0} in the presence of a small B_{y0}(= 0.1) and evolve into a more asymmetric pattern as the guide field B_{y0} increases. (3) The profile of B_y component becomes of a unipolar variation as B_{y0} reaches or exceeds 0.3. As seen in the case of $B_{y0} = 0.5$, a B_y bulge appears in the positive signature of B_y when the enhanced B_y regions caused by Hall effect take place in the plasmoid. The B_y bulge grows into a peaking signature, whose maximum ($B_y|_{max}$) is quickly raised due to the interaction between Hall effect and the additional B_y flux and approaches the lobe magnetic field strength. Such a significant enhancement of the out-of-plane component B_y in the central region of plasmoid might be representative of the observed strong core field in MFR. (4) The plasma inflow might play an important role in generating the link between compressed plasma density and magnetic islands during reconnection; however, the compression of plasma density could be restricted due to the growth of core B_y field.

[29] The following conclusions can be drawn from the above results. (1) Hall effect and a preexisting cross-tail

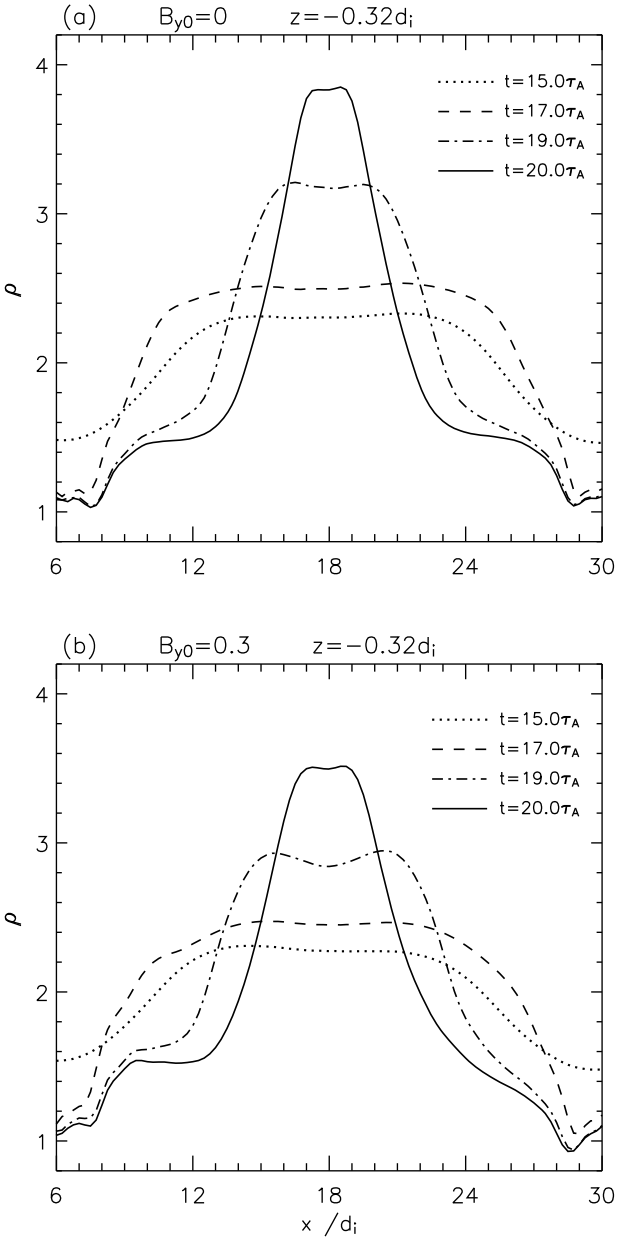

Figure 16. The profiles of plasma density ρ along x at $z = -0.32d_i$ at four different times (a) for Case 1 ($B_{y0} = 0$) and (b) for Case 4 ($B_{y0} = 0.3$).

component B_y are two important factors controlling the occurrence of various plasmoid-like structures in the magnetotail. (2) In the second phase the nonlinear interaction between Hall effect and the additional B_y flux can make a greater contribution than the simple accumulation of the B_y flux fed by the plasma inflow to the growth of the core B_y field. (3) The development of core B_y field in the plasmoid could restrict the compression of plasma density.

[30] **Acknowledgments.** We would like to thank Y. Q. Hu for the helpful discussions and the two reviewers for their helpful suggestions. The work is supported by projects 40674084, 40574061, 40725013, and 40890162 of the National Natural Science Foundation of China.

[31] Wolfgang Baumjohann thanks Vladimir Semwnovich Semenov and another reviewer for their assistance in evaluating this paper.

References

Birn, J., et al. (2001), Geospace Environmental Modeling (GEM) Magnetic Reconnection Challenge, *J. Geophys. Res.*, *106*(A3), 3715–3719.

Chen, L. J., et al. (2007), Observation of energetic electrons within magnetic islands, *Nature Phys.*, *4*, 19–23, doi:10.1038/nphys777.

Daughton, W., J. Scudder, and H. Karimabadi (2006), Fully kinetic simulations of undriven magnetic reconnection with open boundary conditions, *Phys. Plasmas*, *13*, 072101, doi:10.1063/1.2218817.

Deng, X. H., H. Matsumoto, H. Kojima, T. Mukai, R. R. Anderson, W. Baumjohann, and R. Nakamura (2004), Geotail encounter with reconnection diffusion region in the Earth's magnetotail: Evidence of multiple X lines collisionless reconnection?, *J. Geophys. Res.*, *109*, A05206, doi:10.1029/2003JA010031.

Drake, J. F., M. A. Shay, W. Thongthai, and M. Swisdak (2005), Production of energetic electrons during magnetic reconnection, *Phys. Rev. Lett.*, *94*(9), 095001, doi:10.1103/PhysRevLett.94.095001.

Drake, J. F., M. Swisdak, K. M. Schoeffler, B. N. Rogers, and S. Kobayashi (2006), Formation of secondary islands during magnetic reconnection, *Geophys. Res. Lett.*, *33*, L13105, doi:10.1029/2006GL025957.

Eastwood, J. P., D. G. Sibeck, J. A. Slavin, M. L. Goldstein, B. Lavraud, M. Sitnov, S. Imber, A. Balogh, E. A. Lucek, and I. Dandouras (2005), Observations of multiple X-line structure in the Earth's magnetotail current sheet: A Cluster case study, *Geophys. Res. Lett.*, *32*, L11105, doi:10.1029/2005GL022509.

Fu, X. R., Q. M. Lu, and S. Wang (2006), The process of electron acceleration during collisionless magnetic reconnection, *Phys. Plasmas*, *13*, 012309, doi:10.1063/1.2164808.

Hu, Y. Q. (1989), A multistep implicit scheme for time-dependent 2-dimensional magnetohydrodynamic flows, *J. Comput. Phys.*, *84*(10), 441–460.

Huba, J. D. (2005), Hall magnetic reconnection: Guide field dependence, *Phys. Plasmas*, *12*(1), 012322, doi:10.1063/1.1834592.

Ieda, A., A. Machida, T. Mukai, Y. Saito, T. Yamamoto, A. Nishida, T. Terasawa, and S. Kokubun (1998), Statistical analysis of the plasmoid evolution with Geotail observations, *J. Geophys. Res.*, *103*, 4453–4465.

Jin, S. P., and H. L. Cui (2004), The evolution of magnetic helicity in driven reconnection processes and the flux rope structures at the dayside magnetopause, *Phys. Plasmas*, *11*(5), 1816–1824, doi:10.1063/1.1699323.

Jin, S. P., X. P. Hu, Q. G. Zong, S. Y. Fu, B. Wilken, and J. Büchner (2001), A 2.5 dimensional MHD simulation of multiple-plasmoid-like structures in the course of a substorm, *J. Geophys. Res.*, *106*(A12), 29,807–29,830.

Jin, S. P., H. A. Yang, and X. G. Wang (2005), Hall effect and fine structures in magnetic reconnection with high plasma β, *Phys. Plasmas*, *12*(4), 042902, doi:10.1063/1.1870003.

Karimabadi, H., D. Krauss-Varban, N. Omidi, and H. X. Vu (1999), Magnetic structure of the reconnection layer and core field generation in plasmoids, *J. Geophys. Res.*, *104*(A6), 12,313–12,326.

Karimabadi, H., J. D. Huba, D. Krauss-Varban, and N. Omidi (2004), On the generation and structure of the quadrupole magnetic field in the reconnection process: Comparative simulation study, *Geophys. Res. Lett.*, *31*, L07806, doi:10.1029/2004GL019553.

Lee, L. C., Z. F. Fu, and S.-I. Akasofu (1985), A simulation study of forced reconnection processes and magnetospheric storms and substorms, *J. Geophys. Res.*, *90*, 10,896–10,910.

Lui, A. T. Y. (1984), Characteristics of the cross-tail current in the Earth's magnetotail, in *Magnetospheric Currents*, *Geophys. Monogr. Ser.*, vol. 28, edited by T. A. Potemra, pp. 158–170, AGU, Washington, D. C.

Lui, A. T. Y., M. W. Dunlop, H. Rème, L. M. Kistler, G. Gustafsson, and Q.-G. Zong (2007), Internal structure of a magnetic flux rope from Cluster observations, *Geophys. Res. Lett.*, *34*, L07102, doi:10.1029/2007GL029263.

Ma, Z. W., A. Otto, and L. C. Lee (1994), Core magnetic field enhancement in single X line, multiple X line and patchy reconnection, *J. Geophys. Res.*, *99*, 6125–6136.

Moldwin, M. B., and W. Hughes (1992), On the formation and evolution of plasmoids: A survey of ISEE 3 Geotail data, *J. Geophys. Res.*, *97*, 19,259–19,282.

Moldwin, M. B., and W. Hughes (1993), Geomagnetic substorm association of plasmoids, *J. Geophys. Res.*, *98*, 81–88.

Slavin, J. A., et al. (1989), CDAW 8 observations of plasmoid signatures in the geomagnetic tail: An assessment, *J. Geophys. Res.*, *94*(A11), 15,153–15,175.

Slavin, J. A., C. J. Owen, M. M. Kuznetsova, and M. Hesse (1995), ISEE 3 observations of plasmoids with flux rope magnetic topologies, *Geophys. Res. Lett.*, *22*, 2061–2064.

Slavin, J. A., et al. (2003), Cluster electric current density measurements within a magnetic flux rope in the plasma sheet, *Geophys. Res. Lett.*, *30*(7), 1362, doi:10.1029/2002GL016411.

Sonnerup, B. U. Ö. (1987), On the stress balance in flux- transfer events, *J. Geophys. Res.*, *92*, 8613–8620.

Walker, R. J., and T. Ogino (1996), A globle magnetohydrodynamic simulation of the origin and evolution of magnetic flux ropes in the magnetotail, *J. Geomagn. Geoelectr.*, *48*, 765–779.

Yang, H. A., and S. P. Jin (2004), Effects of Hall current in the driven reconnection with various scales, *Chin. Phys. Lett.*, *21*(7), 1394–1397.

Yang, H. A., S. P. Jin, and G. C. Zhou (2006), Density depletion and Hall effect in magnetic reconnection, *J. Geophys. Res.*, *111*, A11223, doi:10.1029/2005JA011536.

Yang, H. A., S. P. Jin, and C. X. Liu (2008), Hall MHD reconnection with an innitial guide field B_{y0}, *Adv. Space Res.*, *41*, 1649–1657, doi:10.1016/j.asr.2007.09.035.

Zong, Q.-G., et al. (1997), Geotail observations of energetic ion species and magnetic field in plasmoid-like structures in the course of an isolated substorm event, *J. Geophys. Res.*, *102*(A6), 11,409–11,428.

S. P. Jin, C. X. Liu, and Q. M. Lu, School of Earth and Space Sciences, University of Science and Technology of China, Hefei 230026, China. (spjin@ustc.edu.cn)

F. S. Wei, State Key Laboratory of Space Weather, Center for Space Science and Applied Research, Chinese Academy of Sciences, Beijing 100080, China.

H. A. Yang, Space Science Center, University of New Hampshire, Durham, NH 03824, USA.